

Floquet generation of magnonic NOON state

Shi-fan Qi¹ and Jun Jing^{1,*}

¹*School of Physics, Zhejiang University, Hangzhou 310027, Zhejiang, China*

(Dated: August 8, 2022)

We propose a concise and deterministic protocol to generate NOON states in a hybrid system consisting of a superconducting qubit, a circuit resonator mode, and two magnon modes, based on the Floquet engineering. In particular, we construct a time-reversal-symmetry broken Hamiltonian for the chiral state propagation of the three continuous-variable modes depending on the qubit state, by the time modulation over the qubit-resonator interaction and the magnon frequency. Then an arbitrary magnonic NOON state can be generated by a typical preparing-and-measurement procedure. We analysis the robustness of our protocol against the systematic errors in the qubit-magnon coupling strength, the Floquet-driving intensity, and the counter-rotating interactions. We can obtain a high-fidelity NOON state in the presence of the quantum dissipation on all components.

I. INTRODUCTION

The NOON states, $(|N0\rangle + |0N\rangle)/\sqrt{2}$ with N integer, consisting of two symmetric components in the maximal superposition [1] are a prominent class of highly entangled states [2]. They have been widely used in quantum metrology [3], quantum communication [4], and quantum information processing [5]. The NOON-state generation [6–15] are conventionally developed on various Rabi oscillations. In practice, they have been realized in multiple quantum platforms, including the polarization states of photons [16], the nuclear spin of molecules [17], the optical paths of photons [18], the superconducting circuits [6, 8], and the phonons in ion traps [19]. The ultra-precise control over the complex quantum devices and the decoherence of quantum systems [20], however, make it extremely difficult to have a large N for a NOON state. It remains therefore interesting to find fast and faithful approaches to generate the NOON states in low-decoherence systems. Here we propose a protocol to realize a magnonic NOON state by virtue of the chiral state transfer based on the Floquet engineering.

The magnonic system is a growing field of research on magnetic devices that operate in the quantum realm. With unique properties such as large tunability, long coherent-time, and strong dipole-dipole coupling to the microwave photons, phonons, and qubits, the magnonic modes have been used as the information carrier in an even broader variety of hybrid systems [21, 22]. They are thus capable to prepare and manipulate various non-classical states [23–31]. Bell states of the magnon-photon system can be generated in both theory proposal [32] and experimental demonstration [33]. Analogous to the cavity quantum electrodynamics [34], Ref. [35] proposed a magnonic cat-state generation protocol, in which the magnon was directly and quantum-coherently coupled to a superconducting transmon qubit.

In a broader view, the NOON states are categorized to the nonclassical states in form of $(|\varphi\rangle|0\rangle + |0\rangle|\varphi\rangle)/\sqrt{2}$,

where $|\varphi\rangle$ is an arbitrary normalized pure state. They can result from a chiral state transfer depending on the symmetrically superposed state of a two-state system in charge of control. Chirality [36, 37] has been found to play an important role in the fractional quantum Hall effect [38] in the magnetic materials. It breaks the time reversal symmetry [39] and realizes the perfect directional state transfer [40, 41]. In recent experiments [42, 43] on superconducting circuits and qubits, the three-spin interaction with chirality is fabricated by the specially designed Floquet driving. Floquet engineering by fast periodic modulation over the characteristic frequency of a quantum system is a major control approach to the desired effective Hamiltonian for the long-time dynamics of the system [44–47]. Also it has been implemented to realize quantum switch [48], chiral ground state current [40], and quantum simulation [49].

In this work, we consider a hybrid qubit-resonator-magnon system upon a state-of-the-art device, in which the qubit is coupled to the resonator mode with time-modulated strength [40, 50] and simultaneously coupled to two magnonic modes [35]. The Floquet engineering is applied to the frequencies of the magnon modes [51]. Exploiting appropriate frequencies, intensities, and phases in control, we can fabricate an effective time-reversal-symmetry broken Hamiltonian to ensure the chiral state transfer amongst the resonator and the two magnonic modes. The transfer direction depends on the state of the qubit. A magnonic NOON state can thus be generated upon preparing the resonator mode as a Fock state $|N\rangle$.

The rest part of this work is structured as follows. In Sec. II, we introduce the full Hamiltonian for the hybrid qubit-resonator-magnon system and then derive an effective Hamiltonian for a perfect chiral state-transfer amongst the three continuous-variable components. In Sec. III, we discuss the systematic errors from the qubit-magnon coupling strength, the Floquet driving intensity, and the counter-rotating interactions. The NOON-state generation protocol and its fidelity analysis are presented in Sec. IV A and Sec. IV B, respectively. The whole work is summarized in Sec. V.

* jingjun@zju.edu.cn

II. MODEL AND CHIRAL STATE TRANSFER

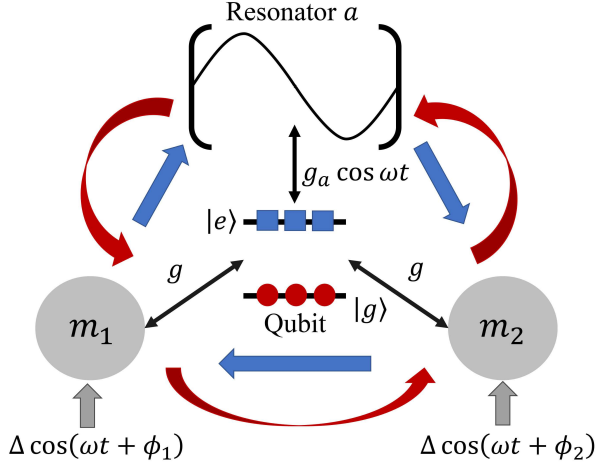


FIG. 1. Diagram of the chiral state propagations amongst the three continuous-variable modes a , m_1 , and m_2 in the hybrid qubit-resonator-magnon system. The population of the qubit on its excited and ground states determines respectively the clockwise and anticlockwise directions of the chiral state propagation.

Consider a hybrid system that consists of a circuit resonator, a superconducting qubit, and two YIG spheres in their ground state (the Kittel mode of the spin ensemble), as shown in Fig. 1. These components are supposed to be resonant with each other in the microwave regime. The qubit-resonator interaction and the frequencies of the two magnonic modes are under the Floquet engineering [40, 50, 51]. Then in the rotating frame with respect to the free Hamiltonian, the full Hamiltonian can be written as

$$H = g_a \cos(\omega t) (\sigma^+ a + \sigma^- a^\dagger) + \Delta \sum_{k=1}^2 \cos(\omega t + \phi_k) m_k^\dagger m_k + g \sum_{k=1}^2 (\sigma^+ m_k + \sigma^- m_k^\dagger), \quad (1)$$

where a (a^\dagger) and m_k (m_k^\dagger) are the annihilation (creation) operators for the resonator mode and the k th magnonic mode, respectively, and $\sigma^+ \equiv |e\rangle\langle g|$ and $\sigma^- \equiv |g\rangle\langle e|$ are the Pauli transition operators. The qubit-resonator interaction is characterized by the coupling strength g_a and the driving frequency ω [40, 50]. For magnons, Δ , ω , and ϕ_k represent the Floquet driving intensity, frequency, and the local phases, respectively [51]. g is the qubit-magnon coupling strength [35].

In the rotating frame with respect to the magnon Hamiltonian under driving [the second term in Eq. (1)], we have

$$H(t) = g_a \cos(\omega t) (\sigma^+ a + \sigma^- a^\dagger) + g \sum_{k=1}^2 \left(e^{if[\sin \phi_k - \sin(\omega t + \phi_k)]} \sigma^+ m_k + \text{H.c.} \right), \quad (2)$$

where $f \equiv \Delta/\omega$. According to the perturbative expansion ordered by the Bessel functions of the first kind, i.e., $e^{iz \sin y} = \sum_{n=-\infty}^{+\infty} J_n(z) e^{iny}$, we have

$$H_I = H_a (e^{i\omega t} + e^{-i\omega t}) + H_0 + \sum_{k=1}^2 \sum_{n=1}^{\infty} \left[H_n^{(k)} e^{in\omega t} + H_{-n}^{(k)} e^{-in\omega t} \right], \quad (3)$$

where

$$H_a = \frac{g_a}{2} (\sigma^+ a + \sigma^- a^\dagger), \\ H_0 = g J_0(f) \sum_{k=1}^2 (\sigma^+ m_k + \sigma^- m_k^\dagger), \\ H_n^{(k)} = g e^{-if \sin \phi_k} e^{in\phi_k} J_n(f) \sigma^- m_k^\dagger + (-1)^n g e^{if \sin \phi_k} e^{in\phi_k} J_n(f) \sigma^+ m_k. \quad (4)$$

Note $H_{-n}^{(k)}$ is the Hermitian conjugate of $H_n^{(k)}$. Using the James' method [45, 46], the interaction Hamiltonian H_I can therefore be written as

$$H_I \approx H_0 + \frac{1}{\omega} \sum_{k=1}^2 \left\{ [H_a, H_{-1}^{(k)}] + [H_1^{(k)}, H_a] \right\} + \sum_{k=1}^2 \frac{1}{n\omega} \sum_{n=1}^{\infty} [H_n^{(k)}, H_{-n}^{(3-k)}], \quad (5)$$

up to the order of $\mathcal{O}(1/\omega^2)$. The zeroth-order term determines that the effective coupling-strength between the magnonic modes and the qubit becomes $g J_0(f)$ under the Floquet driving, which can be tuned by varying the ratio of the driving intensity and frequency, i.e., $f = \Delta/\omega$. This qubit-independent term can be eliminated by setting $J_0(f) = 0$, i.e., $f \approx 2.4048$. In this situation, we have a qubit-dependent effective Hamiltonian

$$H_{\text{eff}} = \sigma_z \left[a^\dagger (g_1 e^{if \sin \phi_1} m_1 + g_2 e^{if \sin \phi_2} m_2) - ig_{12} e^{if(\sin \phi_2 - \sin \phi_1)} m_1^\dagger m_2 + \text{H.c.} \right], \quad (6)$$

where the coupling strengths read

$$g_k = -\frac{g_a g}{\omega} J_1(f) \cos \phi_k, \quad k = 1, 2, \\ g_{12} = \frac{2g^2}{\omega} \sum_{n=1}^{\infty} \frac{J_n^2(f)}{n} \sin [n(\phi_2 - \phi_1)]. \quad (7)$$

To render a perfect chiral transfer amongst the three modes a , m_1 and m_2 , it is required that $|g_1| = |g_2| = |g_{12}| = g_{\text{eff}}$, i.e., $|\cos(\phi_1)| = |\cos(\phi_2)|$. It implies the distinction between driving the coupling strength and driving the frequency in realizing the three-body chirality. When employing the Floquet engineering on the three components' frequency, their phases have to be uniformly distributed in $[0, 2\pi]$. While in our protocol, the phases

are not fixed. A non-unique solution is $\phi_1 = 2\pi/3$ and $\phi_2 = 4\pi/3$, and then

$$g_a = \frac{4g}{J_1(f)} \sum_{n=1}^{\infty} \frac{J_n^2(f)}{n} \sin\left(\frac{2n\pi}{3}\right). \quad (8)$$

Consequently, the effective Hamiltonian in Eq. (6) could be written in a Matrix-product formation,

$$H_{\text{eff}} = g_{\text{eff}} \sigma_z \times \left[a^\dagger, m_1^\dagger, m_2^\dagger \right] \begin{bmatrix} 0 & e^{\frac{i\sqrt{3}f}{2}} & e^{-\frac{i\sqrt{3}f}{2}} \\ e^{-\frac{i\sqrt{3}f}{2}} & 0 & -ie^{-i\sqrt{3}f} \\ e^{\frac{i\sqrt{3}f}{2}} & ie^{i\sqrt{3}f} & 0 \end{bmatrix} \begin{bmatrix} a \\ m_1 \\ m_2 \end{bmatrix}, \quad (9)$$

which is convenient to obtain the evolution of these continuous-variable operators

$$\begin{bmatrix} a(t) \\ m_1(t) \\ m_2(t) \end{bmatrix} = \hat{T}(t) \begin{bmatrix} a(0) \\ m_1(0) \\ m_2(0) \end{bmatrix}. \quad (10)$$

Here $\hat{T}(t)$ depends on the state of the qubit. When the qubit is in the excited state $|e\rangle$, we have

$$\hat{T}(t) = \hat{T}^{(e)}(t) = \frac{1}{3} \begin{bmatrix} x(t) & -ie^{\frac{i\sqrt{3}f}{2}}y(t) & ie^{-\frac{i\sqrt{3}f}{2}}z(t) \\ ie^{-\frac{i\sqrt{3}f}{2}}z(t) & x(t) & -e^{-i\sqrt{3}f}y(t) \\ -ie^{\frac{i\sqrt{3}f}{2}}y(t) & -e^{-i\sqrt{3}f}z(t) & x(t) \end{bmatrix}, \quad (11)$$

where

$$\begin{aligned} x(t) &= 1 + 2 \cos\left(\sqrt{3}g_{\text{eff}}t\right), \\ y(t) &= 1 + 2 \cos\left(\sqrt{3}g_{\text{eff}}t - \frac{2\pi}{3}\right), \\ z(t) &= 1 + 2 \cos\left(\sqrt{3}g_{\text{eff}}t + \frac{2\pi}{3}\right). \end{aligned} \quad (12)$$

The transformation matrix $\hat{T}^{(e)}$ entails a sufficient condition for a clockwise and periodic chirality. It is interesting to find that $m_2(t) = a(0)$, $m_1(t) = m_2(0)$, and $a(t) = m_1(0)$ when $t = (2\pi/3 + 2n\pi)/(\sqrt{3}g_{\text{eff}})$; $m_2(t) = m_1(0)$, $m_1(t) = a(0)$, and $a(t) = m_2(0)$ when $t = (4\pi/3 + 2n\pi)/(\sqrt{3}g_{\text{eff}})$; and $m_k(t) = m_k(0)$, $a(t) = a(0)$ when $t = 2n\pi/(\sqrt{3}g_{\text{eff}})$ with n integer. This transfer is exactly the rotation $a \rightarrow m_2 \rightarrow m_1 \rightarrow a$ described by the straight-line arrows in Fig. 1, corresponding to a clockwise chiral propagation of states in the Schrödinger picture, i.e., $|\varphi_a\varphi_1\varphi_2\rangle \rightarrow |\varphi_1\varphi_2\varphi_a\rangle \rightarrow |\varphi_2\varphi_1\varphi_a\rangle$, where $|\varphi_a\rangle$ and $|\varphi_k\rangle$ are arbitrary states for the resonator and magnonic mode- k , respectively.

Consider the resonator is prepared as an arbitrary superposed state $C_n|n\rangle$ and the two magnonic modes are in their ground states, i.e.,

$$|\varphi(0)\rangle = \sum_n C_n|n00\rangle = \sum_n \frac{C_n}{\sqrt{n!}} [a^\dagger(0)]^n |000\rangle. \quad (13)$$

By virtue of Eq. (11), it is straightforward to express the time-evolved state as

$$|\varphi(t)\rangle = \sum_n \frac{C_n}{\sqrt{n!}} \left[\sum_{j=1}^3 a^\dagger(0) \hat{T}_{j1}^{(e)}(t) \right]^n |000\rangle. \quad (14)$$

For example, when $|\varphi(0)\rangle = |100\rangle$, we have

$$|\varphi(t)\rangle = \frac{1}{3} \left[x(t)|100\rangle + ie^{-\frac{i\sqrt{3}f}{2}}z(t)|010\rangle - ie^{\frac{i\sqrt{3}f}{2}}y(t)|001\rangle \right]. \quad (15)$$

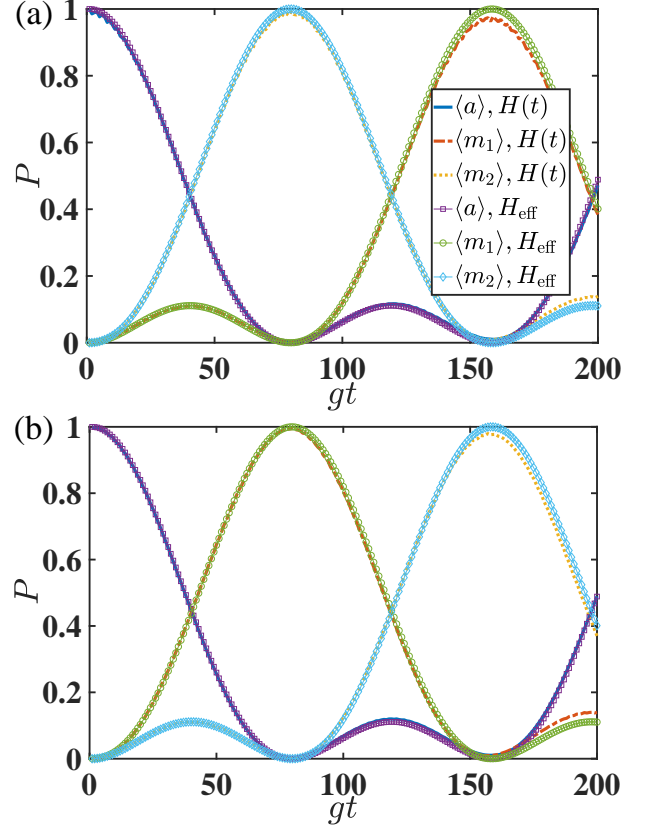


FIG. 2. The chiral dynamics of the state populations P_j , $j = a, 1, 2$, for the three modes by the numerical simulation with the Floquet engineering Hamiltonian (1) and the analytical evaluation with the effective Hamiltonian (6). In (a), the qubit is at $|e\rangle$ and in (b), it is at $|g\rangle$. The resonator-mode a is initialized as $|1\rangle$. The parameters are set as $\omega = 20g$, $\phi_1 = 2\pi/3$, and $\phi_2 = 4\pi/3$.

We can have a unit transfer fidelity at the desired moments for the general superposed state in Eq. (13), e.g., when $t = 2\pi/(3\sqrt{3}g_{\text{eff}})$, $|\varphi(t)\rangle = \sum_n C_n|00n\rangle$. To avoid the influence from the local phases [52] during the whole evolution, the state-transfer fidelity can be measured by the time-dependent state populations

$$P_j(t) = \sum_{C_n \neq 0} |\langle \varphi(t) | n \rangle_j|^2, \quad (16)$$

where $|n\rangle_j$, $j = a, 1, 2$, indicates that the marked mode is in the Fock state $|n\rangle$ and the other two modes are in their ground states.

In parallel to Eq. (11), we have

$$\hat{T}(t) = \hat{T}^{(g)}(t) = \frac{1}{3} \begin{bmatrix} x(t) & -ie^{\frac{i\sqrt{3}f}{2}}z(t) & ie^{-\frac{i\sqrt{3}f}{2}}y(t) \\ ie^{-\frac{i\sqrt{3}f}{2}}y(t) & x(t) & -e^{-i\sqrt{3}f}z(t) \\ -ie^{\frac{i\sqrt{3}f}{2}}z(t) & -e^{-i\sqrt{3}f}y(t) & x(t) \end{bmatrix}, \quad (17)$$

when the qubit is in the ground state $|g\rangle$. The transformation matrix $\hat{T}^{(g)}$ indicates an anticlockwise chirality, yielding the transfer along the rotation $a \rightarrow m_1 \rightarrow m_2 \rightarrow a$ described by the curve arrows in Fig. 1. Then in the Schrödinger picture, a chiral evolution emerges as $|\varphi_a\varphi_1\varphi_2\rangle \rightarrow |\varphi_2\varphi_a\varphi_1\rangle \rightarrow |\varphi_1\varphi_2\varphi_a\rangle$. For the same initial states in Eq. (13), by virtue of Eq. (17), we have

$$|\varphi(t)\rangle = \sum_n \frac{C_n}{\sqrt{n!}} \left[\sum_j a^\dagger(0) \hat{T}_{j1}^{(g)}(t) \right]^n |000\rangle. \quad (18)$$

Figures 2(a) and 2(b) show the time-evolved state populations $P_j(t)$ under the effective Hamiltonian (6) (see the lines with markers) and the system Hamiltonian in Eq. (1) (see the lines with no markers), demonstrating the respective clockwise and anticlockwise chirality. The numerical and analytical results are found to match perfectly with each other. The chiral direction is fully determined by the qubit state. The period of the chiral state propagation is state-independent and calculated by the coupling strengths in Eq. (7) under the condition $J_0(f) = 0$.

III. SYSTEMATIC ERRORS

In practice, the ideal chiral state transfer in Fig. 2 using the effective Hamiltonian (6) cannot be exactly realized because of the imperfections and constraints in experiments. Even under the desired conditions in the last section, i.e., fast engineering, exact cancellation of the undesired term, and accurate setting of the coupling strength, the systematic errors pose the need to estimate the perturbation effect on the transport protocols from the stochastic fluctuation in parameters of the full Hamiltonian. In the rest of this section, we analysis the systematic errors induced by the qubit-magnon coupling-strength deviation, the unstable Floquet driving, and the presence of the counter-rotating interactions.

A. The qubit-magnon coupling-strength deviation

The coupling between the qubit and the two magnonic modes [the last term in Eq. (1)] are chosen the same in magnitude. They are practically dependent on the

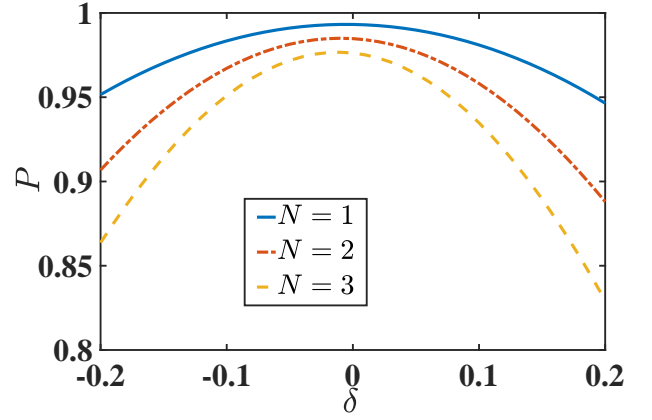


FIG. 3. Chiral state-transfer fidelity of the target state $(|e00N\rangle + |g0N0\rangle)/\sqrt{2}$ as a function of the systematic error associated with the qubit-magnon coupling-strength. Ideally (under the effective Hamiltonian) the initial state $(|eN00\rangle + |gN00\rangle)/\sqrt{2}$ would be faithfully become the target state at the desired moment $t = 2\pi/(3\sqrt{3}g_{\text{eff}})$. Here the parameters are set the same as Fig. 2.

distance between the two YIG spheres and the qubit. We first consider the deviation of these two coupling strengths from a fixed value. The system Hamiltonian can thus be rewritten as

$$H = g_a \cos(\omega t) (\sigma^+ a + \sigma^- a^\dagger) + \Delta \cos(\omega t + \phi_1) m_1^\dagger m_1 + g(1 + \delta) (\sigma^+ m_1 + \sigma^- m_1^\dagger) + \Delta \cos(\omega t + \phi_2) m_2^\dagger m_2 + g(1 - \delta) (\sigma^+ m_2 + \sigma^- m_2^\dagger), \quad (19)$$

where δ represents the magnitude of the relative error. Under the same settings that $\phi_1 = 2\pi/3$, $\phi_2 = 4\pi/3$, $J_0(f = \Delta/\omega) = 0$, and $|g_k| = |g_{12}|$ in Eq. (7) for the chiral transfer, the effective Hamiltonian in Eq. (9) is modified by changing the coefficient matrix into

$$g_{\text{eff}} \begin{bmatrix} 0 & (1 + \delta)e^{\frac{i\sqrt{3}f}{2}} & (1 - \delta)e^{-\frac{i\sqrt{3}f}{2}} \\ (1 + \delta)e^{-\frac{i\sqrt{3}f}{2}} & 0 & -i(1 - \delta^2)e^{-i\sqrt{3}f} \\ (1 - \delta)e^{\frac{i\sqrt{3}f}{2}} & i(1 - \delta^2)e^{i\sqrt{3}f} & 0 \end{bmatrix}. \quad (20)$$

The dynamics under the nonideal Hamiltonian (19) can be presented in Fig. 3 by the sensitivity of the transfer fidelity (population) of the target state $|\Phi(t)\rangle = (|e00N\rangle + |g0N0\rangle)/\sqrt{2}$ that evolves from the initial state $|\Phi(0)\rangle = (|eN00\rangle + |gN00\rangle)/\sqrt{2}$, to the systematic error δ . The populations are evaluated at the desired time, that is determined by the ideal chiral state-transfers depending on Eqs. (11) and (17). Note H_{eff} is the result of the second-order perturbation of H . So that one can find a less-than-unit population even when $\delta = 0$. The state-transfer population in general declines with increasing $|\delta|$ and N . Our protocol is robust since even under $|\delta| \approx 20\%$ and $N = 3$, the population is still about 0.85.

B. The unstable Floquet driving

To cancel the qubit-independent dynamics of the whole system to realize a chiral propagation of quantum states, the ratio $f = \Delta/\omega$ of the Floquet-driving intensity Δ and the frequency ω is set to meet the requirement $J_0(f) = 0$ in Sec. II. We now estimate the effect of the control error arising from the unstable Floquet-driving intensity. The Hamiltonian in Eq. (1) can thus be modified to

$$\begin{aligned}
 H = & g_a \cos(\omega t) (\sigma^+ a + \sigma^- a^\dagger) \\
 & + \Delta \sum_{k=1}^2 (1 + \epsilon_k) \cos(\omega t + \phi_k) m_k^\dagger m_k \\
 & + g \sum_{k=1}^2 (\sigma^+ m_k + \sigma^- m_k^\dagger).
 \end{aligned} \tag{21}$$

where ϵ_k indicates a dimensionless random fluctuations for the driving intensity on the magnonic mode- k . It is assumed to be in the range of $[0, \epsilon]$ with $\epsilon < 1$.

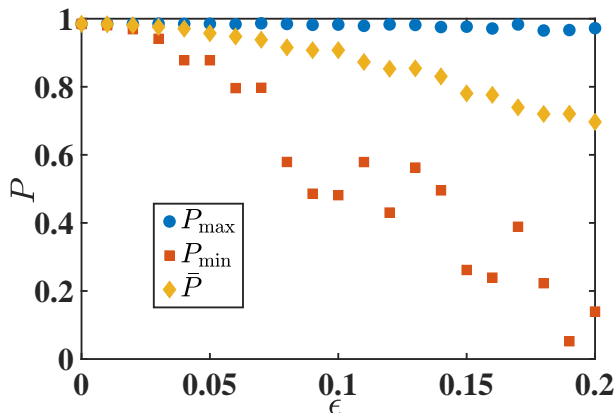


FIG. 4. Chiral state-transfer fidelity of the target state $(|e002\rangle + |g020\rangle)/\sqrt{2}$ as a function of the systematic error associated with the Floquet-driving intensity. The circles, squares, and diamonds represent the maximum P_{\max} , minimum P_{\min} , and average populations \bar{P} , respectively. Here the parameters are set the same as Fig. 2.

In Fig. 4, we present the sensitivity of the state-transfer population to the error upperbound ϵ . The initial state is chosen as $|\Phi(0)\rangle = (|e200\rangle + |g200\rangle)/\sqrt{2}$ and then the target state is $|\Phi[t = 2\pi/(3\sqrt{3}g_{\text{eff}})]\rangle = (|e002\rangle + |g020\rangle)/\sqrt{2}$. The results, including the maximum P_{\max} , the minimum P_{\min} , and the average values \bar{P} , are obtained by performing 100 numerical simulations using randomly distributed ϵ_k 's. The distance between P_{\max} and P_{\min} is found to decrease roughly with increasing ϵ . The average population \bar{P} can be maintained above 0.90 when $\epsilon \leq 0.1$, and above 0.70 when $\epsilon \leq 0.2$. However, the minimum value P_{\min} declines to below 0.50 when ϵ approaches 0.1. It implies the dramatic error caused by the fluctuation in the Floquet driving intensity, which is more significant than that in the qubit-magnon coupling-strength.

C. The presence of the counter-rotating interaction

Back to the lab frame, the full Hamiltonian under the resonant condition is written as

$$\begin{aligned}
 H' = & \omega_a (a^\dagger a + \sigma^+ \sigma^-) \\
 & + \sum_{k=1}^2 [\omega_a + \Delta \cos(\omega t + \phi_k)] m_k^\dagger m_k \\
 & + g_a \cos(\omega t) (\sigma^+ a + \sigma^- a^\dagger + \sigma^+ a^\dagger + \sigma^- a) \\
 & + \sum_{k=1}^2 g (\sigma^+ m_k + \sigma^- m_k^\dagger + \sigma^+ m_k^\dagger + \sigma^- m_k),
 \end{aligned} \tag{22}$$

where ω_a represents the characteristic frequency of the four components. The system Hamiltonian H in Eq. (1) for our chiral state-transfer protocol is obtained in the rotating frame with respect to the free Hamiltonian involving ω_a and valid in the rotating-wave approximation. It means that both qubit-magnon and qubit-resonator coupling strengths g_a and g have to be much smaller than the transition frequency ω_a in magnitude. Although a faster speed of the chiral transfer demands uniquely a larger g_a or g , a constrain condition for $|g|$ has to be considered by including the counter-rotating interactions to the original Hamiltonian H' .

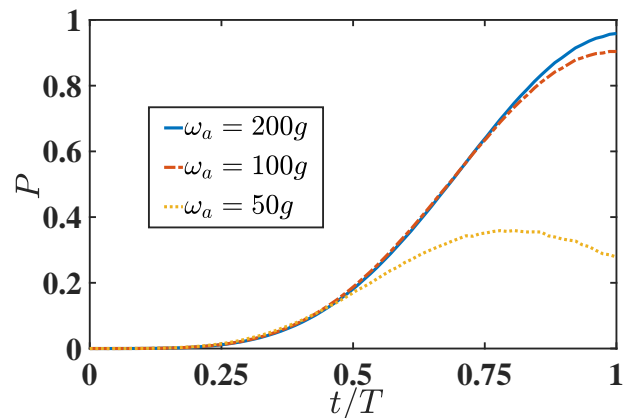


FIG. 5. Time evolution of the chiral state-transfer fidelity of the target state $(|e002\rangle + |g020\rangle)/\sqrt{2}$ under various transition-frequency ω_a . The other parameters are the same as Fig. 2.

Figure 5 could be used to estimate the implicitly required magnitude of ω_a to justify the system Hamiltonian H in our protocol. We demonstrate the effect of the counter-rotating interactions by the chiral state-transfer population dynamics from the initial state $|\Phi(0)\rangle = (|e200\rangle + |g200\rangle)/\sqrt{2}$ under various transition frequency ω_a . It is found that the population can be maintained above 0.90 when $\omega_a = 100g$ and above 0.98 when $\omega_a = 200g$. A smaller ω_a yields a lower P . When ω_a decreases to $\omega_a = 50g$, P is lower than 0.30 in the end of the evolution with $T = 2\pi/(3\sqrt{3}g_{\text{eff}})$.

IV. NOON STATE GENERATION AND FIDELITY ANALYSIS

This section devotes to the steps of generating the magnonic NOON states based on the Floquet-engineering Hamiltonian (1) under the qubit-dependent chiral-transfer condition. Also we analysis the protocol fidelity in the presence of the quantum dissipation.

A. Preparing NOON state with multiple excitations

Suppose that all the four components in our hybrid system (qubit, resonator mode, and two magnonic modes) are initially in their ground states, i.e., $|\Phi(0)\rangle = |g000\rangle = |g\rangle_q |0\rangle_a |0\rangle_{m_1} |0\rangle_{m_2}$. The generation procedure of the magnonic NOON state could be constituted by two parts, part *A* and part *B*.

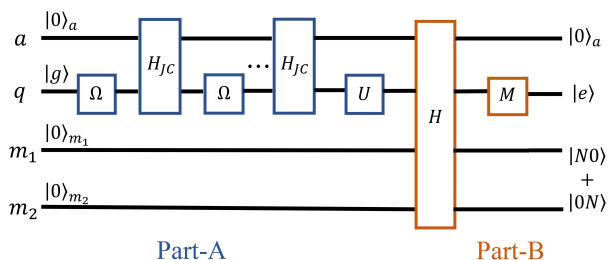


FIG. 6. Circuit model of the magnonic NOON state generation. Part *A* is used to prepare the resonator as a Fock state $|N\rangle$ and the qubit to be a symmetrical-superposed state. It consists of a sequence of π -pulses on qubit characterized by the frequency Ω and the local evolution of qubit and resonator under a Jaynes-Cummings Hamiltonian H_{JC} (23) and ends up with a $\pi/2$ -pulse U (26) on qubit. In Part *B*, after the global evolution under the Floquet-engineering Hamiltonian (1), a projective measurement is performed on qubit to either of its bare basis.

As illustrated by the circuit model in Fig. 6, Part *A* is mainly used to prepare the resonator mode as an arbitrary Fock state $|N\rangle$. Accordingly, it is divided into $N+1$ steps as following. This part is local to the resonator and the qubit. Then to avoid the unnecessary crosstalk with the two magnons, the resonator and the qubit are tuned to be far-off-resonant from them. And we temporally remove the time-modulation over the coupling strength between the qubit and the resonator. Thus in Part *A* we have a Jaynes-Cummings Hamiltonian

$$H_{JC} = g_a (\sigma^+ a + \sigma^- a^\dagger). \quad (23)$$

Step A₁. A microwave π -pulse of $\{\omega_q, \pi/(2\Omega)\}$ is applied to the qubit and the system state is transformed to $|\Phi(\tau)\rangle = |e000\rangle$ up to a global phase. Here ω_q is the pulse frequency, which is currently resonant with the qubit. $\tau \equiv \pi/(2\Omega)$ is the duration time of the pulse. The Rabi frequency Ω is assumed to be much larger than

g_a to make it reasonable to ignore the evolution under H_{JC} during a sufficiently short τ . Then turning on the Hamiltonian (23) for a period of $\tau_1 = \pi/(2g_a)$, we have

$$|\Phi(\tau + \tau_1)\rangle = -|g100\rangle. \quad (24)$$

Step A_j, $j = 2, \dots, N$. We alternatively employ the same microwave π -pulse $\{\omega_q, \pi/(2\Omega)\}$ to pump the qubit from the ground state to the excited state and switches on and off the Hamiltonian (23) with a decreasing duration time $\tau_j = \pi/(2\sqrt{j}g_a)$ to transform $|e(j-1)00\rangle$ to be $|gj00\rangle$. Therefore after these steps, the system state becomes

$$|\Phi(T_A)\rangle = (-1)^N |gN00\rangle, \quad (25)$$

where $T_A = N\tau + \sum_{j=1}^N \tau_j$. Till now, a number state is created in the resonator mode. The global phase $(-1)^N$ can be ignored for simplicity.

Step A_{N+1}. A $\pi/2$ -pulse gate U is performed on the qubit. It can be expressed as

$$U = e^{i(\pi/4)\vec{\sigma}\cdot\vec{n}} = \frac{1}{\sqrt{2}} \begin{bmatrix} 1 & ie^{-i\theta} \\ ie^{i\theta} & 1 \end{bmatrix}, \quad (26)$$

where $\vec{\sigma} \equiv (\sigma_x, \sigma_y, \sigma_z)$ and $\vec{n} = (\cos \theta, \sin \theta, 0)$. The qubit becomes a superposed state and the system state reads,

$$|\Phi(T_A)\rangle = \frac{1}{\sqrt{2}} (|g\rangle + ie^{i\theta}|e\rangle) |N00\rangle, \quad (27)$$

where the phase θ is tunable as desired and determines the final local phase of the NOON state.

In the beginning of Part *B*, we are well-prepared to generate the magnonic NOON state based on the full Hamiltonian (1) and the system state in Eq. (27).

Step B₁. Under the desired time-modulations over the qubit-resonator interaction and the Floquet engineering over the magnonic modes to achieve the effective Hamiltonian in Eq. (6), the system state evolves to

$$|\Phi(T_A + T)\rangle = \frac{1}{\sqrt{2}} (|g0N0\rangle - ie^{i\theta}|e00N\rangle), \quad (28)$$

after $T = 2\pi/(3\sqrt{3}g_{\text{eff}})$, according to the transformation matrices in Eqs. (11) and (17). Then we detune the qubit-frequency and apply a microwave $\pi/2$ -pulse $\{\omega_q, \pi/(4\Omega)\}$ to the qubit. The state becomes

$$\begin{aligned} & |\Phi(T_B = T_A + T + \tau/2)\rangle \\ &= \frac{1}{2} (|g0N0\rangle - e^{i\theta}|g00N\rangle) - \frac{i}{2} (|e0N0\rangle + e^{i\theta}|e00N\rangle) \\ &= \frac{1}{2} |g0\rangle (|N0\rangle - e^{i\theta}|0N\rangle) - \frac{i}{2} |e0\rangle (|N0\rangle + e^{i\theta}|0N\rangle). \end{aligned} \quad (29)$$

Step B₂. In the last step, one can obtain the magnonic NOON state $(|N0\rangle - e^{i\theta}|0N\rangle)/\sqrt{2}$ or $(|N0\rangle + e^{i\theta}|0N\rangle)/\sqrt{2}$ by performing a projective measurement on the ground or the excited state of the qubit. To hold the NOON state,

the frequencies of all the four components can then be off-set to avoid unnecessary evolution.

In a general situation, an arbitrary state $|\varphi\rangle$ initialized in the resonator mode can be used to generate the entangled state $(|\varphi\rangle|0\rangle + |0\rangle|\varphi\rangle)/\sqrt{2}$ of the two magnonic modes through Part *B*. For example, if the resonator mode is initialized as a coherent state $|\alpha\rangle$, then the result is an entangled coherent state [53] of two magnonic modes, $(|\alpha\rangle|0\rangle + |0\rangle|\alpha\rangle)/\sqrt{2}$.

B. Fidelity Analysis

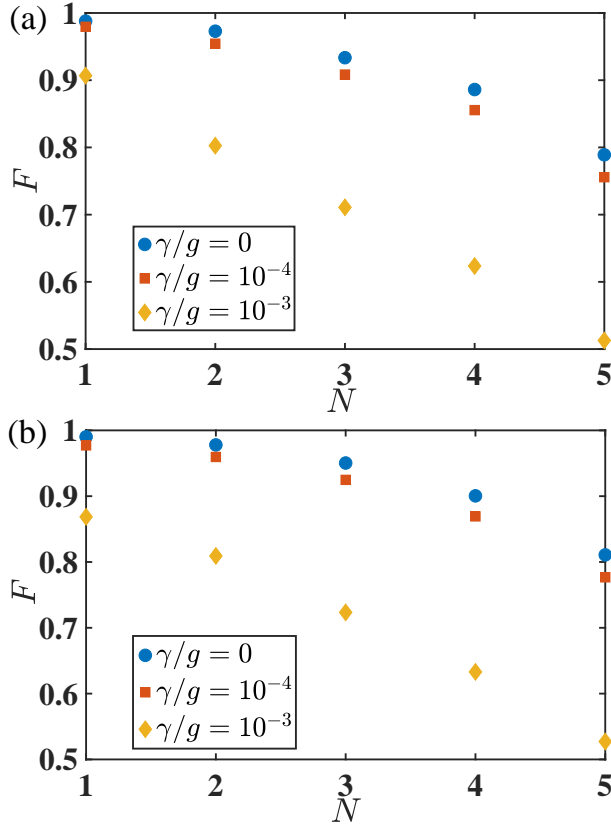


FIG. 7. Fidelity of the NOON state obtained by the projective measurement over (a) the excited state and (b) the ground state of the qubit (see *Step B₂*), under various decoherence rate γ . Here the parameters are set as $\omega = 20g$, $\phi_1 = 2\pi/3$, $\phi_2 = 4\pi/3$, $\theta = \pi$, and $\Omega = 30g$.

The generation protocol could be verified by the numerical simulation over the whole procedure in Sec. IV A. The overlap of the final state and the ideal NOON state in the end of *Step B₂* could be regarded as the generation-protocol fidelity. In particular, we prepare the whole system as the separable ground state, follow all the steps in Part *A* and Part *B*, and take account the decoherence from all components of the hybrid system into the dynamics. Under the standard Markovian approximation and tracing out the degrees of freedom of the external

environment (assumed to be at the vacuum state), we arrive at the master equation for the density-matrix operator $\rho(t)$ of the whole system consisting of qubit, resonator, and magnonic modes:

$$\dot{\rho}(t) = -i \left[\tilde{H}, \rho(t) \right] + \kappa_a \mathcal{L}[a]\rho(t) + \kappa_m \mathcal{L}[m_1]\rho(t) + \kappa_m \mathcal{L}[m_2]\rho(t) + \gamma \mathcal{L}[\sigma^-]\rho(t). \quad (30)$$

In Part *A* for the local evolution of qubit and resonator, $\tilde{H} = H_{\text{JC}}$ (23); in Part *B* for the global evolution, $\tilde{H} = H$ (1). κ_a , κ_m , and γ are the decoherence rates of the resonator, the magnonic modes, and the qubit, respectively. To simplify the discussion but with no loss of generality, we set $\kappa_a = \kappa_m = \gamma$. These rates are surely dependent on the magnitude of the associated transitions in spontaneous emission. Yet this setting is simply used to estimate the robustness of the ideal protocol, so all of the decoherence rates are supposed to be in the same order of magnitude. The dissipative superoperator \mathcal{L} is defined in a Lindblad form,

$$\mathcal{L}[o] \equiv \frac{1}{2} (2o\rho o^\dagger - o^\dagger o \rho - \rho o^\dagger o), \quad (31)$$

where $o = \sigma^-, a, m_1, m_2$ are the decay operators.

Using Eq. (29), *Step B₂*, and Eq. (30), the fidelity is calculated by $F = \langle \Psi | \text{Tr}_{\text{qr}}[\rho(T_B)] | \Psi \rangle$, where $|\Psi\rangle$ is the target NOON state and Tr_{qr} means tracing out the degrees of freedom of qubit and resonator. Performing $|e\rangle\langle e|$ and $|g\rangle\langle g|$ on $|\Phi(T_B)\rangle$ gives rise to $|\Psi\rangle = (|N0\rangle + e^{i\theta}|0N\rangle)/\sqrt{2}$ and $|\Psi\rangle = (|N0\rangle - e^{i\theta}|0N\rangle)/\sqrt{2}$, respectively. In Fig. 7, we plot the fidelity of the NOON state under various decoherence rates γ . As expected, the fidelities decline with the increasing N . The result is not sensitive to the choice of the measurement basis in comparison Figs. 7(a) and 7(b). With a moderate decoherence rate $\gamma/g = 10^{-4}$, the fidelities are 97.9%, 95.4%, 90.1%, 85.6%, and 75.6% for $N = 1, 2, 3, 4, 5$ in Fig. 7(a) by projection to the excited state $|e\rangle$. And they are respectively 97.8%, 96.0%, 92.4%, 86.9%, and 77.7% in Fig. 7(b) by measuring the ground state. Roughly the latter are slightly higher than the former and both demonstrate robustness against the environmental dissipation. Under a strong decoherence rate $\gamma/g = 10^{-3}$, however, the generation fidelity will decline near to 50%.

V. CONCLUSION

In summary, we have proposed a magnonic NOON state generation protocol based on the Floquet engineering method. The control protocol is carried out in a hybrid qubit-resonator-magnon system, where the qubit is coupled to the resonator mode with a time-modulation interaction and simultaneously coupled to two magnonic modes. The Floquet engineering with desired driving intensity, frequency, and local phases is applied to the

eigen-frequencies of two magnons, by which an effective time-reversal-symmetry broken Hamiltonian is constructed to realize a chiral state transfer amongst the resonator and the two magnonic modes. The state transfer direction could be controlled by the state of the qubit. In our protocol, when the qubit is prepared as $(|e\rangle + |g\rangle)/\sqrt{2}$, an arbitrary pure state (including the Fock state) of the resonator can thus be symmetrically transferred to the two magnons at the same time. We can eventually obtain the magnonic NOON state upon a projective measurement on qubit. We estimate the sensitivity of the state-transfer fidelity to the systematic errors in the qubit-magnon coupling strength, the Floquet driving

intensity, and the counter-rotating interactions. Our protocol shows robustness against the quantum dissipation of all the components. Our work provides an alternative approach to generate NOON state in a novel hybrid system, which constitutes an interesting application of chiral state transfer under Floquet control.

ACKNOWLEDGMENTS

We acknowledge financial support from the National Science Foundation of China (Grants No. 11974311 and No. U1801661).

-
- [1] A. N. Boto, P. Kok, D. S. Abrams, S. L. Braunstein, C. P. Williams, and J. P. Dowling, *Quantum interferometric optical lithography: Exploiting entanglement to beat the diffraction limit*, *Phys. Rev. Lett.* **85**, 2733 (2000).
- [2] R. Horodecki, P. Horodecki, M. Horodecki, and K. Horodecki, *Quantum entanglement*, *Rev. Mod. Phys.* **81**, 865 (2009).
- [3] L. Pezzè, A. Smerzi, M. K. Oberthaler, R. Schmied, and P. Treutlein, *Quantum metrology with nonclassical states of atomic ensembles*, *Rev. Mod. Phys.* **90**, 035005 (2018).
- [4] N. Gisin and R. Thew, *Quantum communication*, *Nat. Photon.* **1**, 165 (2007).
- [5] C. Bennett and B. DiVincenzo, *Quantum information and computation*, *Nature* **404**, 247 (2000).
- [6] F. W. Strauch, K. Jacobs, and R. W. Simmonds, *Arbitrary control of entanglement between two superconducting resonators*, *Phys. Rev. Lett.* **105**, 050501 (2010).
- [7] S. T. Merkel and F. K. Wilhelm, *Generation and detection of noon states in superconducting circuits*, *New J. Phys.* **12**, 3175 (2010).
- [8] H. Wang, M. Mariantoni, R. C. Bialczak, M. Lenander, E. Lucero, M. Neeley, A. D. O'Connell, D. Sank, M. Weides, J. Wenner, T. Yamamoto, Y. Yin, J. Zhao, J. M. Martinis, and A. N. Cleland, *Deterministic entanglement of photons in two superconducting microwave resonators*, *Phys. Rev. Lett.* **106**, 060401 (2011).
- [9] Q. P. Su, C. P. Yang, and S. B. Zheng, *Fast and simple scheme for generating noon states of photons in circuit qed*, *Sci. Rep.* **4**, 3898 (2014).
- [10] S. J. Xiong, Z. Sun, J. M. Liu, T. Liu, and C. P. Yang, *Efficient scheme for generation of photonic noon states in circuit qed*, *Opt. Lett.* **40**, 2221 (2015).
- [11] Q.-P. Su, H.-H. Zhu, L. Yu, Y. Zhang, S.-J. Xiong, J.-M. Liu, and C.-P. Yang, *Generating double noon states of photons in circuit qed*, *Phys. Rev. A* **95**, 022339 (2017).
- [12] S.-f. Qi and J. Jing, *Generating noon states in circuit qed using a multiphoton resonance in the presence of counter-rotating interactions*, *Phys. Rev. A* **101**, 033809 (2020).
- [13] M. D'Angelo, A. Garuccio, and V. Tamma, *Toward real maximally path-entangled n-photon-state sources*, *Phys. Rev. A* **77**, 063826 (2008).
- [14] K. Kamide, Y. Ota, S. Iwamoto, and Y. Arakawa, *Method for generating a photonic noon state with quantum dots in coupled nanocavities*, *Phys. Rev. A* **96**, 013853 (2017).
- [15] G. Vanhaele, A. Bäcker, R. Ketzmerick, and P. Schlagheck, *Creating triple-noon states with ultracold atoms via chaos-assisted tunneling*, *Phys. Rev. A* **106**, L011301 (2022).
- [16] Y. Israel, S. Rosen, and Y. Silberberg, *Supersensitive polarization microscopy using noon states of light*, *Phys. Rev. Lett.* **112**, 103604 (2014).
- [17] J. A. Jones, S. D. Karlen, J. Fitzsimons, S. C. Ardan, A. Benjamin, A. D. Briggs, and J. J. L. Morton, *Magnetic field sensing beyond the standard quantum limit using 10-spin noon states*, *Science* **324**, 1166 (2009).
- [18] I. Afek, O. Ambar, and Y. Silberberg, *High-noon states by mixing quantum and classical light*, *Science* **328**, 879 (2010).
- [19] J. Zhang, M. Um, D. Lv, J.-N. Zhang, L.-M. Duan, and K. Kim, *Noon states of nine quantized vibrations in two radial modes of a trapped ion*, *Phys. Rev. Lett.* **121**, 160502 (2018).
- [20] J. Chen and L. F. Wei, *Deterministic generations of photonic noon states in cavities via shortcuts to adiabaticity*, *Phys. Rev. A* **95**, 033838 (2017).
- [21] D. Lachance-Quirion, Y. Tabuchi, A. Glorpe, K. Usami, and Y. Nakamura, *Hybrid quantum systems based on magnonics*, *Appl. Phys. Express* **12**, 070101 (2019).
- [22] Y. Li, W. Zhang, V. Tyberkevych, W. K. Kwok, and V. Novosad, *Hybrid magnonics: physics, circuits, and applications for coherent information processing*, *J. Appl. Phys.* **128**, 130902 (2020).
- [23] O. O. Soykal and M. E. Flatté, *Strong field interactions between a nanomagnet and a photonic cavity*, *Phys. Rev. Lett.* **104**, 077202 (2010).
- [24] O. O. Soykal and M. E. Flatté, *Size dependence of strong coupling between nanomagnets and photonic cavities*, *Phys. Rev. B* **82**, 104413 (2010).
- [25] J. Li, S.-Y. Zhu, and G. S. Agarwal, *Magnon-photon-phonon entanglement in cavity magnomechanics*, *Phys. Rev. Lett.* **121**, 203601 (2018).
- [26] Y.-P. Wang, G.-Q. Zhang, D. Zhang, T.-F. Li, C.-M. Hu, and J. Q. You, *Bistability of cavity magnon polaritons*, *Phys. Rev. Lett.* **120**, 057202 (2018).
- [27] X. Zhang, C.-L. Zou, L. Jiang, and H. Tang, *Cavity magnonmechanics*, *Sci. Adv.* **2**, e1501286 (2016).
- [28] Y. Tabuchi, S. Ishino, A. Noguchi, T. Ishikawa, R. Yamazaki, K. Usami, and Y. Nakamura, *Coherent coupling*

- between a ferromagnetic magnon and a superconducting qubit, *Science* **349**, 405 (2015).
- [29] D. Lachance-Quirion, S. Piotr Wolski, Y. Tabuchi, S. Kono, K. Usami, and Y. Nakamura, *Entanglement-based single-shot detection of a single magnon with a superconducting qubit*, *Science* **367**, 425 (2020).
- [30] Y. Tabuchi, S. Ishino, T. Ishikawa, R. Yamazaki, K. Usami, and Y. Nakamura, *Hybridizing ferromagnetic magnons and microwave photons in the quantum limit*, *Phys. Rev. Lett.* **113**, 083603 (2014).
- [31] X. Zhang, C.-L. Zou, L. Jiang, and H. X. Tang, *Strongly coupled magnons and cavity microwave photons*, *Phys. Rev. Lett.* **113**, 156401 (2014).
- [32] S.-f. Qi and J. Jing, *Generation of bell and greenberger-horne-zeilinger states from a hybrid qubit-photon-magnon system*, *Phys. Rev. A* **105**, 022624 (2022).
- [33] H. Y. Yuan, P. Yan, S. Zheng, Q. Y. He, K. Xia, and M.-H. Yung, *Steady bell state generation via magnon-photon coupling*, *Phys. Rev. Lett.* **124**, 053602 (2020).
- [34] A. Blais, A. L. Grimsmo, S. M. Girvin, and A. Wallraff, *Circuit quantum electrodynamics*, *Rev. Mod. Phys.* **93**, 025005 (2021).
- [35] M. Kounalakis, G. E. W. Bauer, and Y. M. Blanter, *Analog quantum control of magnonic cat states on a chip by a superconducting qubit*, *Phys. Rev. Lett.* **129**, 037205 (2022).
- [36] P. Lodahl, S. Mahmoodian, S. Stobbe, A. Rauschenbeutel, P. Schneeweiss, J. Volz, H. Pichler, and P. Zoller, *Chiral quantum optics*, *Nature* **541**, 473 (2017).
- [37] H. Zhu, J. Yi, M.-Y. Li, J. Xiao, L. Zhang, C.-W. Yang, R. A. Kaindl, L.-J. Li, Y. Wang, and X. Zhang, *Observation of chiral phonons*, *Science* **359**, 579 (2018).
- [38] A. S. Sørensen, E. Demler, and M. D. Lukin, *Fractional quantum hall states of atoms in optical lattices*, *Phys. Rev. Lett.* **94**, 086803 (2005).
- [39] J. Koch, A. A. Houck, K. L. Hur, and S. M. Girvin, *Time-reversal-symmetry breaking in circuit-qed-based photon lattices*, *Phys. Rev. A* **82**, 043811 (2010).
- [40] P. Roushan, C. Neill, A. Megrant, Y. Chen, R. Babbush, R. Barends, B. Campbell, Z. Chen, B. Chiaro, A. Dunsworth, A. Fowler, E. Jeffrey, J. Kelly, E. Lucero, J. Mutus, P. ÓMalley, M. Neeley, C. Quintana, D. Sank, A. Vainsencher, J. Wenner, T. White, E. Kapit, H. Neven, and J. Martinis, *Chiral ground-state currents of interacting photons in a synthetic magnetic field*, *Nat. Phys.* **13**, 146 (2017).
- [41] D.-W. Wang, H. Cai, R.-B. Liu, and M. O. Scully, *Mesoscopic superposition states generated by synthetic spin-orbit interaction in fock-state lattices*, *Phys. Rev. Lett.* **116**, 220502 (2016).
- [42] D.-W. Wang, C. Song, W. Feng, and et al., *Synthesis of antisymmetric spin exchange interaction and chiral spin clusters in superconducting circuits*, *Nat. Phys.* **15**, 382 (2019).
- [43] W. Liu, W. Feng, W. Ren, D.-W. Wang, and H. Wang, *Synthesizing three-body interaction of spin chirality with superconducting qubits*, *Appl. Phys. Lett.* **116**, 114001 (2020).
- [44] N. Goldman and J. Dalibard, *Periodically driven quantum systems: Effective hamiltonians and engineered gauge fields*, *Phys. Rev. X* **4**, 031027 (2014).
- [45] W. Shao, C. Wu, and X.-L. Feng, *Generalized james' effective hamiltonian method*, *Phys. Rev. A* **95**, 032124 (2017).
- [46] M. Bukov, L. D'Alessio, and A. Polkovnikov, *Universal high-frequency behavior of periodically driven system: from dynamical stabilization to floquet engineering*, *Adv. in Phys.* **64**, 139 (2015).
- [47] F. Petiziol, M. Sameti, S. Carretta, S. Wimberger, and F. Mintert, *Quantum simulation of three-body interactions in weakly driven quantum systems*, *Phys. Rev. Lett.* **126**, 250504 (2021).
- [48] Y. Wu, L.-P. Yang, M. Gong, Y. Zheng, H. Deng, Z. Yan, Y. Zhao, K. Huang, A. D. Castellano, W. J. Munro, K. Nemoto, D.-N. Zheng, C. Sun, Y.-x. Liu, X. Zhu, and L. Lu, *An efficient and compact switch for quantum circuits*, *npj. Quantum Inf.* **4**, 50 (2018).
- [49] O. Kyriienko and A. S. Sørensen, *Floquet quantum simulation with superconducting qubits*, *Phys. Rev. Applied* **9**, 064029 (2018).
- [50] S. D. Liberato, C. Ciuti, and I. Carusotto, *Quantum vacuum radiation spectra from a semiconductor microcavity with a time-modulated vacuum rabi frequency*, *Phys. Rev. Lett.* **98**, 103602 (2007).
- [51] J. Xu, C. Zhong, X. Han, D. Jin, L. Jiang, and X. Zhang, *Floquet cavity electromagnonics*, *Phys. Rev. Lett.* **125**, 237201 (2020).
- [52] S.-f. Qi and J. Jing, *Accelerated adiabatic passage in cavity magnomechanics*, *Phys. Rev. A* **105**, 053710 (2022).
- [53] B. C. Sanders, *Entangled coherent states*, *Phys. Rev. A* **45**, 6811 (1992).